

# Carbon Nanotubes Toxicity

Stefano Bellucci

**Abstract** We describe current and possible future developments in nanotechnology for biological and medical applications. Nanostructured, composite materials for drug delivery, biosensors, diagnostics and tumor therapy are reviewed as examples, placing special emphasis on silica composites. Carbon nanotubes are discussed as a primary example of emerging nanomaterials for many of the above-mentioned applications. Toxicity effects of this novel nanomaterial are discussed and the need for further study of potential hazards for human health, professionally exposed workers and the environment is motivated.

## 1 Introduction

The purpose of nanotechnology is not merely creating useful or functional materials and devices by manipulating matter at the nanometer length scale, but most importantly exploiting novel properties of materials which arise just owing to the nanoscale. Simply meeting the length scale criterion of 1–100 nm is not really nanotechnology, rather it is a necessary condition; the corresponding sufficient condition consists in taking advantage of novel (physical, chemical, mechanical, electrical, optical, magnetic, etc.) properties that result solely because of going from bulk to the nanoscale.

Since 2001, when the U.S. announced a National Nanotechnology Initiative (NNI) aimed at creating a dedicated program to explore nanotechnology (see <http://www.nano.gov/>), many other countries, including the EU (see e.g. <http://www.euronanoforum2007.eu/>), Japan (see [www.nanonet.go.jp](http://www.nanonet.go.jp)), China (see e.g. <http://www.sipac.gov.cn>), followed up with their own nanotechnology research programs. It is important to recall the special character of nanotechnology as a both pervasive and enabling technology, with potential impact in all sectors of the economy: Electronics, computing, data storage, materials and manufacturing, health and medicine,

---

Stefano Bellucci

INFN-Laboratori Nazionali di Frascati, Via E. Fermi 40, 00044 Frascati, Italy,  
e-mail: [bellucci@lnf.infn.it](mailto:bellucci@lnf.infn.it)

energy, transportation, environment, national security, space exploration and others. In this article, we focus on nanotechnology applications in the biomedical sector.

Carbon nanotubes (CNTs) are an example of a carbon-based nanomaterial [1], which has won enormous popularity in nanotechnology for its unique properties and applications [2]. CNTs have physicochemical properties that are highly desirable for use within the commercial, environmental, and medical sectors. With the inclusion of CNTs to improve the quality and performance of many widely used products, as well as potentially in medicine, it is likely that occupational and public exposure to CNT-based nanomaterials will increase dramatically in the near future. Hence, it is of the utmost importance to explore the yet almost unknown issue of the toxicity of this new material. Here, we compare the toxicity of pristine and oxidized multi-walled carbon nanotubes on human T cells and find that the latter are more toxic and induce massive loss of cell viability through programmed cell death at doses of  $400\mu\text{g/ml}$ , which corresponds to approximately 10 million carbon nanotubes per cell. Pristine, hydrophobic, carbon nanotubes were less toxic and a ten-fold lower concentration of either carbon nanotube type was not nearly as toxic. Our results suggest that carbon nanotubes indeed can be very toxic at sufficiently high concentrations and that careful toxicity studies need to be undertaken particularly in conjunction with nanomedical applications of carbon nanotubes.

## 2 Nanotechnology for Tumor Therapy

Over the past three and a half decades, since the beginning of the U.S. National Cancer Initiative in 1971, there have been major advances in the diagnosis and treatment of cancer. However, the severe toll cancer continues to impose on our society represents one of the major healthcare concerns of our nations. One out of every two men and one out of every three women in their lifetime will be confronted with a cancer diagnosis. Conventional treatments currently rely heavily upon radiation and chemotherapy, which are extremely invasive and painstakingly plagued by very serious side effects. Nanotechnology yields the hope for new methods for a noninvasive therapy, capable of minimizing side effects. One of the promising approaches consists in the targeted destruction of cancerous cells using localized heating.

The use of thermal cancer therapies is beneficial in many respects over the conventional tumor removal by surgery. Indeed, normally, most thermal approaches have a very small degree of invasiveness; they are relatively simple to perform and may enable physicians to treat tumors embedded in vital regions where surgical removal is unfeasible. Ideally, the activating energy to heat the tumor would be targeted on the embedded tumor with minimal effect on surrounding healthy tissue. Unfortunately, conventional heating techniques such as focused ultrasound, microwaves, and laser light do not discriminate between tumors and surrounding healthy tissues. Thus, success has been modest, and typically, treatments result in some damage to surrounding tissue.

Recent work suggests that nanostructures designed to attach to cancerous cells may provide a powerful tool for producing highly localized energy absorption at the sites of cancerous cells. Indeed, work since 2003 at La Charité Hospital in Berlin [3], with scientists at the F. Schiller-Universität Jena, showed that magnetic nanoparticles interstitially injected directly into the tumor, and heated with radio-frequency radiation [4], can destroy cancer cells in a human brain tumor and are also believed to enhance the effects of subsequent radiation therapy. Nanoparticles localize on the tumor due to a special biomolecularly modified outer layer – leaving the surrounding healthy tissue with minimum damage.

In this way, it was proven that iron oxide nanoparticles, with diameters 10,000 times smaller than that of a human hair, can be introduced inside cancer cells and then treated in such a way as to produce a significant damage to tumor cells in order to fight a particularly aggressive form of brain cancer called glioblastoma, although the method can be employed to treat other forms of the disease. The procedure involves coating the iron oxide nanoparticles with an organic substance, such as the sugar glucose, before injecting them into the tumor. Cancer cells, having a fast metabolism and correspondingly high energy needs, are much more eager to eat up the sugar-coated nanoparticles, in comparison with healthy cells, which appear minimally or not at all affected (Fig. 1).

In this selective procedure, the magnetic field is responsible for the heating up of the nanoparticles in the cancerous tissue, reaching temperatures up to 45°C (Fig. 2), with the aim of destroying many of the tumor cells or at least to weaken them to such an extent that conventional methods, e.g. radiation or chemotherapy, can more easily and effectively get rid of them.

The treatment, known as magnetic fluid hyperthermia, was successfully used to prolong the life of laboratory rats which were implanted with malignant brain tumors (Figs. 3 and 4). Rats receiving nanotherapy lived four times as long as rats receiving no treatment.

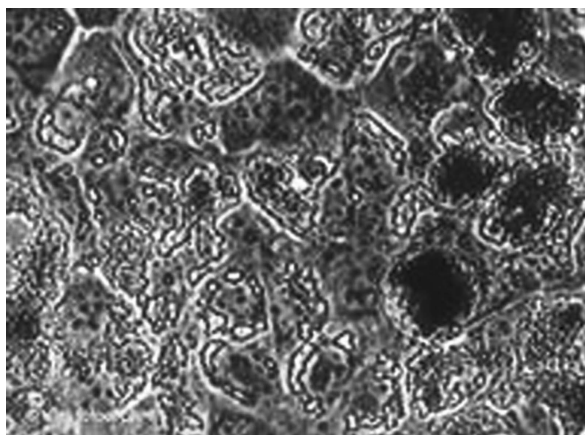


**Fig. 1** The image shows nanoparticles surrounding cancer cells. Image source: MFH Hyperthermiesysteme GmbH and MagForce Applications GmbH, Berlin, Germany

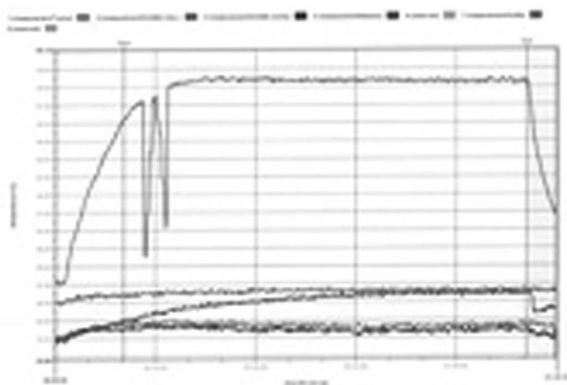


**Fig. 2** The treatment is automatically recorded with the temperature of the tumor (*top curve in the diagram*) and other body-temperatures registered. Image source: MFH Hyperthermiesysteme GmbH and MagForce Applications GmbH, Berlin, Germany

Then, the therapy was given to 15 patients suffering from *Glioblastoma multiforme*, the most common primary brain tumor and the most aggressive form of brain cancer (with a 6–12 months life expectancy prognosis in humans).

The treatment is particularly attractive to doctors working with tumors in the brain since the nanoparticles can be targeted on the cancerous tissue, so that the therapy turns out to be ideal for curing tumors that lie outside the reach of conventional surgical treatment, such as those situated deep in the brain or in regions that are responsible for essential tasks like speech or motor functions.

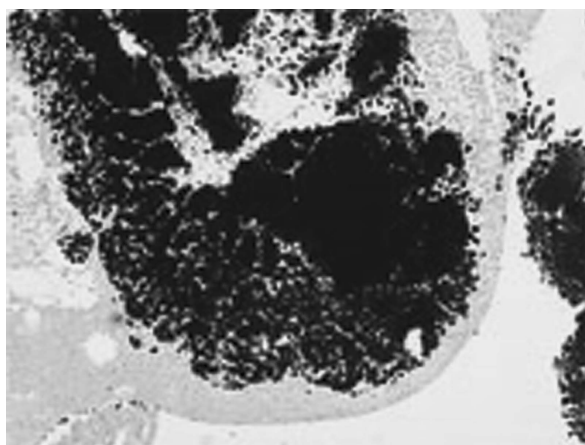


**Fig. 3** In pre-clinical tests, the characteristics of nanoparticles were optimized; shown: accumulation of nanoparticles in tumor tissue (RG-2 glioblastoma of the rat). Image source: MFH Hyperthermiesysteme GmbH and MagForce Applications GmbH, Berlin, Germany

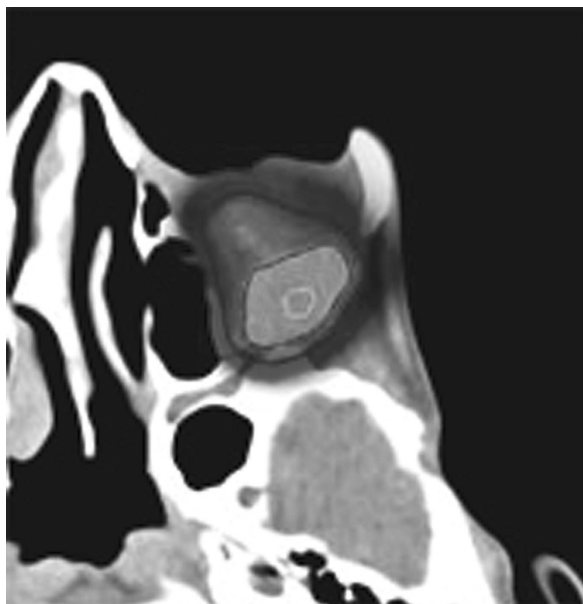


**Fig. 4** A precise thermotherapy of target areas in almost every body region is possible (here, thermotherapy of the orbita up to a maximum temperature of 49°C). Image source: MFH Hyperthermiesysteme GmbH and MagForce Applications GmbH, Berlin, Germany

In principle, the hyperthermia therapy is not limited to just various types of brain cancer. Since breast tumors do not lie in the immediate vicinity of essential organs, one can hope to apply the treatment, heating the cancerous tissue up to yet higher temperatures, in order to get a very effective cure of breast tumor, which may even be combined with parallel treatments relying upon conventional radiation therapy and chemotherapy.

However, one should bear in mind a caveat: keeping the amount of metal injected into the body stay under a certain level is the way to maintain the danger of "nanopoisoning" at a relatively low level. N.B.: After all, it should be remembered that nanoparticles are already used routinely in magnetic resonance therapy for the diagnosis of liver tumors.

After the therapy, nanoparticles do not have to be removed and are slowly metabolized. Since, so far, no harmful side effects from thermotherapy with magnetic nanoparticles could be observed, neither on animals nor on human beings, in 2004 nanoparticles have started to be applied for treating human prostate carcinomas at the Clinic for Urology, Charité – University Medicine, Berlin, Germany.

Moving to countries outside Europe, in order to complete the survey, we observe that in Japan [5], work at Nagoya University with magnetite cationic liposomes (MCLs) combined with heat shock proteins has shown great potential in cancer treatment as well. Using MCLs, one locally generates heat in a tumor by placing test mice in an alternating magnetic field and not cause the body temperature of the test

animal to rise. After injection of MCLs and application of a magnetic field, tumor and body temperature differed by 6°C. The combined treatment strongly inhibited tumor growth over a 30-day period and complete regression of tumors was observed in 20% of the mice.

Finally, in the U.S., researchers at Rice University recently reported work on mice in which gold-coated nanoparticles treated to attach to cancerous cells were heated using infrared radiation. Sources of infrared radiation can be tuned to transmit at a narrow band of electromagnetic frequencies. Additionally, the "nanoshells" size can be changed to absorb a particular infrared radiation frequency. Hence, one can choose a frequency of the infrared radiation that couples with the gold-coated nanoparticles, while at the same time, does not couple with the tissue of the body, thus enabling the selective destruction of cancerous cells and tumors [6]. The results of a preliminary experiment with mice treated with the nanoshells-infrared radiation therapy have proven to be very encouraging.

In conclusion, we can say that progress in nanotherapy, obtained by several groups worldwide, using independent techniques, shows the global interest in nanoscience and its potential application to innovative medical technologies. This justifies the expectation that nanotechnology will soon yield a powerful tool for treating cancer.

### 3 Nanotechnology for Diagnostics and Drug Delivery (The source for the material contained in this section is: Strem Chemicals)

Magnetic nanoparticles have been used as markers in biomedical diagnostics. In fact, due to the fact that bound and unbound nanoparticles have different magnetic relaxation times, biochemical binding reactions can be detected by means of a SQUID-high resolution measurement technique (Fig. 5). Magnetic relaxation immunoassays were realized by means of this technique. Also, in vivo-applications of magneto-relaxometry seem possible, e.g. in cancer diagnostics.

However, the use of magnetic nanoparticles is not limited to the abovementioned applications, but can also be extended for achieving drug or radiation delivery. In particular, small magnetic particles can be engineered to carry therapeutic chemicals

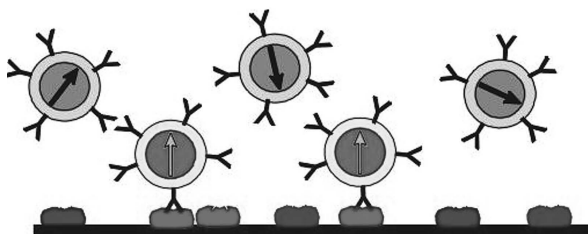


**Fig. 5** Immobilization of magnetic nanoparticles by antibody-antigen coupling (Contact: Dietmar.Eberbeck@ptb.d)

or radiation for tumor control. Because they are magnetic, the particles can be guided by an external magnetic field and can be forced to move with or against the flow of blood in veins or arteries or held in a fixed position once they have been conveyed to a target organ, and possibly retrieved when treatment has ended. Work is in progress at Argonne Nat. Lab. and the University of Chicago.

One is, of course, interested in using biosensors and biolabels to understand living cells. Nanotechnology has the potential to increase our ability to understand the fundamental working of living cells. Many potential applications for nanomaterials as biosensors and biolabels are under investigation. They have found use in cellular studies, enhanced spectroscopic techniques, biochips, and protein and enzyme analysis. Fluorescent nanoparticles can be used for cell labeling and magnetic nanoparticles may be utilized as sensors. Multi-color labeling of both fixed and living cells with fluorescent nanoparticles conjugated with biological ligands that specifically bind against certain cellular targets enables the recording of diffusion pathways in receptor cells.

The uptake of nanoparticles into the vesicular compartments around the nucleus of cells can be used to label the cells so that their pathway and fate can be followed. The nanoparticles exhibit reduced photobleaching as compared to traditional dyes and are passed on to daughter cells during cell division, therefore allowing for much longer term observation. Magnetic nanoparticles can also act as sensors for assessing how external stresses affect changes in intracellular biochemistry and gene expression.

We can ask ourselves, how can nanotechnology improve medical diagnostics? Naturally, the early detection of a disease remains the primary goal of the medical community. Nanotechnology holds great promises for enabling the achievement of this goal. Nanoparticles, in particular, have exhibited tremendous potential for detecting fragments of viruses, pre-cancerous cells, disease markers, and indicators of radiation damage. Biomolecule coated, ultra small, superparamagnetic iron oxide (USPIO) particles injected in the blood stream recognize target molecular markers present inside cells and induce a specific signal for detection by magnetic resonance imaging (MRI). This technology may allow for detection of individual cancer cells months or years earlier than traditional diagnostic tools, which require the presence of hundreds of cancer cells.

In this respect, we can also address the issue of how biobarcode amplification assays (BCA) can use nanoparticles in disease detection. A nanoparticle-based BCA utilizes gold nanoparticles and magnetic microparticles attached to large numbers of DNA strands and antibodies for a specific disease marker. The marker binds to the nano- and microparticles forming a complex that is separated from the sample using a magnetic field. Heating the complexes releases the DNA barcodes, which emit an amplified signal due to their large numbers. This BCA technology has been applied to the detection of markers for Alzheimer's disease and is being investigated for numerous others.

There are also stimulating suggestions that nanotechnology can improve targeted drug delivery. Targeted drug delivery systems can convey drugs more effectively and/or more conveniently, increase patient compliance, extend the product life cycle,

provide product differentiation, and reduce health care costs. Drug delivery systems that rely on nanomaterials also allow for targeted delivery of compounds characterized by low oral bioavailability due to poor water solubility, permeability and/or instability and provide for longer sustained and controlled release profiles. These technologies can increase the potency of traditional small molecule drugs in addition to potentially providing a mechanism for treating previously incurable diseases.

There are many other applications for nanomaterials in the medical and pharmaceutical sector, which we only have the possibility, owing to limitations in the length of these notes, to merely list. Areas currently under investigation include gene therapy, antibacterial/antimicrobial agents for burn and wound dressings, repair of damaged retinas, artificial tissues, prosthetics, enhancing signals for magnetic resonance imaging examinations, and as radio frequency controlled switching of complex biochemical processes.

## 4 Carbon Nanotubes

The development of nanomaterials is currently underway in laboratories worldwide for medical and biotechnological applications including gene delivery [7, 8] drug delivery [9, 10] enzyme immobilization [11, 12] and biosensing. [13, 14]. The most commonly used materials are gold [15], silica and semiconductors. Silica nanoparticles have been widely used for biosensing and catalytic applications due to their large surface area-to-volume ratio, straightforward manufacture, and the compatibility of silica chemistry with covalent coupling of biomolecules [16–18].

A key challenge in nanotechnology is the more precise control of nanoparticle assembly for the engineering of particles with the desired physical and chemical properties. Much research is currently focused on CNT as a promising material for the assembly of nanodevices, based upon new CNT–composite materials, such as CNT with a thin surface cover [19, 20] or CNT bound to nanoparticles [21–24], in order to tailor their properties for specific applications.

In this section, reviewing the results reported in [25], we present the tunable synthesis of multi-walled CNT–silica nanoparticle composite materials. Instead of coupling prefabricated silica nanobeads to CNT, we chose to grow the silica nanobeads directly onto functionalized multi-walled CNT by reaction of tetraethyl- or tetramethyl-orthosilicate (TEOS or TMOS) with a functionalized CNT precursor, prepared by coupling aminopropyltriethoxysilane (APTEOS) to a functionalized multi-walled CNT through a carboxamide bond, using a water-in-oil microemulsion to strictly control the nanobead size.

The body of the ideal multi-walled CNT is formed by several nested and straight cylindrical graphene sheets. In reality, nanotubes usually appear curved and have topological defects. Under strong oxidizing conditions (conc.  $\text{HNO}_3$ ), nanotubes can be cut into shorter and straighter pieces having carboxylic acid groups at both their tips and at imperfections on their walls [26]. We oxidized multi-walled CNT with outer diameters of ca. 20–40 nm and lengths of 5–10  $\mu\text{m}$  (NanoLab, Inc.,



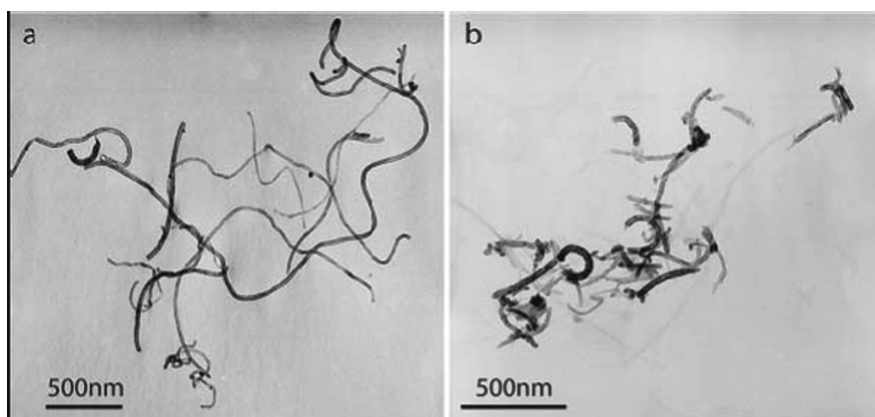


**Fig. 6** Multi-walled carbon nanotubes before (a) and after (b) oxidation in nitric acid

Newton, MA, USA) (Fig. 6a) by refluxing in concentrated  $\text{HNO}_3$  for 6 hours, followed by several washes with distilled water. The oxidized CNT (CNT-COOH) were shorter and straighter (Fig. 6b).

Their carboxylic acid groups greatly facilitated their dispersion in aqueous solutions, as well as their further functionalization (Fig. 7a). A detailed description of the procedure for generating the activated CNT precursor (CNT-APTEOS) to the composite from CNT-COOH by activation of its carboxylic acid groups can be found in [25].

Using the procedure described in [25], we obtained new CNT–nanocomposites consisting of CNT with covalently attached silica nanobeads (Fig. 8). Non-oxidized CNT (with negligible COOH content) did not support any composite formation (not shown). The inverse microemulsion system resulted in nanobeads covalently linked to the CNT only at locations functionalized with triethoxy-silane groups, while the bare graphitic wall of the pristine CNT did not associate with reverse micelles. Transmission electron microscopic (TEM) images revealed morphologies indicative of different nanobead diameters. Small nanoparticles were found to decorate the walls and ends of the CNT prepared using TMOS as precursor (Fig. 8a–c). In many cases, small nanoparticle aggregates were observed to be associated with the CNT (Fig. 8c), as expected for the high density of functional groups on the CNT. Under the conditions used for synthesis of larger nanoparticles, CNT were either decorated by individual nanobeads (Fig. 8d–f) or had a uniform silica coating around the entire CNT (Fig. 8g and h). We also observed some functionalized CNT that appeared to have silica within their tubes (Fig. 8i). The internal presence of silica was not observed with the non-treated nanotubes. Further work is in progress to better understand the filling mechanism.

In summary, we covalently coated carbon nanotubes with silica nanoparticles of different sizes. Perhaps, the most valuable feature of our work [25] is that the architecture of the obtained assemblies can be largely controlled by varying the conditions in the synthesis. Thus, the length of CNT is regulated by the oxidation time

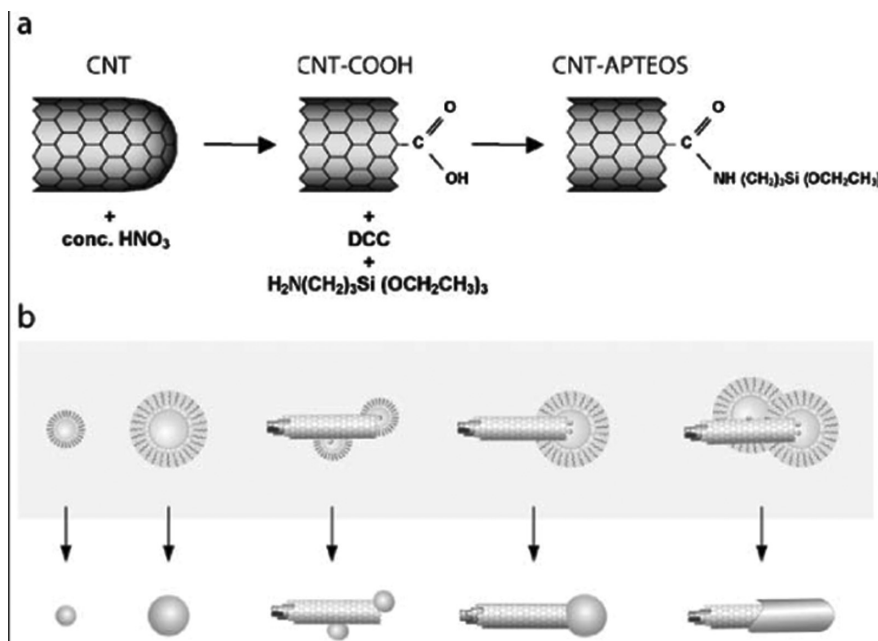


**Fig. 7** Scheme for preparing the CNT-nanoparticle composite. **(a)** Oxidation and preparation of the CNT-APTEOS precursor. **(b)** Formation of silica nanobeads in reverse micelles in a water-in-oil microemulsion. Inclusion of CNT-APTEOS nucleates the formation of nanobeads on the covalently linked propyltriethoxysilane groups (dots inside the micelles) by reaction with TEOS or TMOS

(Fig. 6) and the size of the nanobeads by using microemulsion conditions that yield micelles of a particular size. Indeed, silica nanobeads were prepared in a water-in-oil microemulsion system in which the water droplets served as nanoreactors [27, 28]. The size of the final nanospheres was mainly regulated by the dimension of the water droplets, and therefore, by the molar ratio of water to surfactant ( $w$ ). Smaller nanobeads were prepared by reducing  $w$ . Furthermore, the dimension of the final product can be controlled by varying the molar ratio of water to precursor ( $h$ ), the molar ratio of precursor to catalyst ( $n$ ), by choosing the reactivity of the precursor, and the reaction time and temperature. The values of the variable parameters ( $w, h, n$ ) used can be found in Table 1 of [25].

Because the chemical properties of the silica surface are particularly versatile and silica can be doped with fluorescent [29], magnetic [30] or biological macromolecules [31], nanostructures with a wide range of morphologies suitable for different applications can be obtained. We anticipate that further refinement of our water-in-oil microemulsion approach for creating novel nanostructures combined with procedures for isolating discrete products will allow us to combine different nanostructures into higher order assemblies that could be useful for a variety of applications, including providing an interface between living cells and biosensor arrays.

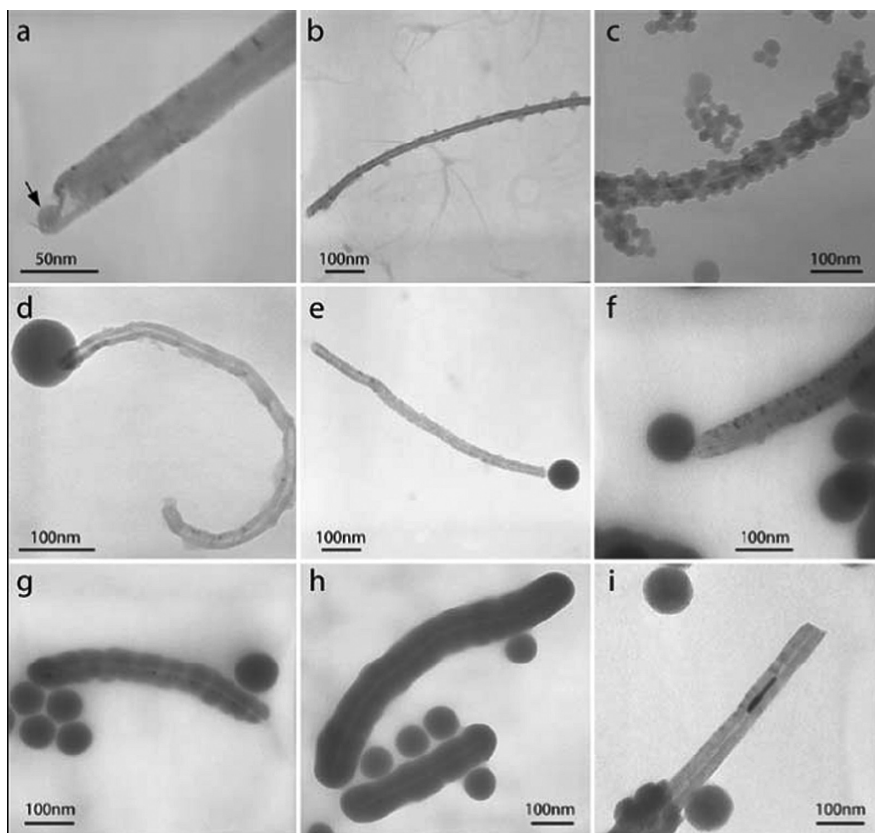


**Fig. 8** TEM images of the CNT-nanocomposites prepared using conditions for small (a–c) or large (d–i) silica nanobeads. The *arrow* in panel (a) indicates a nanobead at the tip of the CNT. The *arrow* in panel (i) indicates a polymerized silica inside a CNT

## 5 Supramolecular Nanostructures

In [32], we constructed and characterized supramolecular nanostructures consisting of ruthenium-complex luminophores, which were directly grafted onto short oxidized single-walled carbon nanotubes or physically entrapped in silica nanobeads, which had been covalently linked to short oxidized single-walled carbon nanotubes or hydrophobically adsorbed onto full-length multi-walled carbon nanotubes. These structures were evaluated as potential electron-acceptor complexes for use in the fabrication of photovoltaic devices, and for their properties as fluorescent nanocomposites for use in biosensors or nanoelectronics.

The carboxylic acid groups of oxidized SWCNT which originated from the nitric acid-oxidation, were covalently tethered to the ruthenium-complexes (Fig. 9A) or luminophore-doped silica nanobeads (Fig. 9B), whereas the full-length MWCNT had the ruthenium complex-doped silica nanobeads introduced onto their surfaces

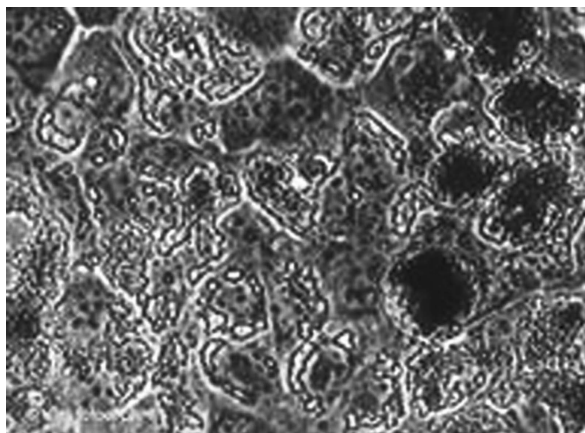


**Fig. 9** Scheme for preparing the supramolecular nanostructures. **A:** Ruthenium-complex luminophores were directly grafted onto oxidized SWCNT to form a supramolecular donor–acceptor nanostructure. **B:** Ruthenium-complex luminophore-doped silica nanobeads were covalently linked to short oxidized SWCNT to form a supramolecular fluorescent nanostructure. **C:** Ruthenium-complex luminophore-doped silica nanobeads were hydrophobically adsorbed onto full-length MWCNT via  $\pi$ – $\pi$  interactions to form a supramolecular fluorescent nanostructure with CNT having the  $\pi$ -electronic structure intact

by hydrophobic adsorption via  $\pi$ – $\pi$  interactions to maintain the intact CNT  $\pi$ -electronic structure.

The absorbance spectrum of  $\text{Ru}(\text{ap})(\text{bpy})_2$  in DMF exhibited a narrow peak at approximately 289 nm, which we attribute to a ligand-to-ligand  $\pi \rightarrow \pi^*$  transition, and by two broad bands at approximately 375 and 460 nm, which we attribute to  $d_{\text{Ru}} \rightarrow \pi^*$  ligand singlet metal-to-ligand charge-transfer transitions (Fig. 10A). On excitation at 460 nm, the steady state emission of  $\text{Ru}(\text{ap})(\text{bpy})_2$  in DMF revealed an emission band centered at 606-nm (Fig. 10B).

The absorbance spectrum of  $\text{Ru}(\text{ap})(\text{bpy})_2$ -decorated SWCNT dissolved in DMF was broad and slightly blue-shifted compared to that from  $\text{Ru}(\text{ap})(\text{bpy})_2$  in DMF to confirm that luminophores decorated the nanotube surface (Fig. 10A). The spectroscopic contribution of  $\text{Ru}(\text{ap})(\text{bpy})_2$  grafted onto SWCNT was calculated by subtracting from the absorbance spectrum of the nanostructure that of oxidized SWCNT (dissolved in DMF), with matching absorption at 900 nm, because the spectroscopic contribution of the luminophore was absent for that wavelength. The peaks in the calculated absorbance spectrum of  $\text{Ru}(\text{ap})(\text{bpy})_2$  grafted on SWCNT were centered at the same wavelengths and slightly broader compared to those of  $\text{Ru}(\text{ap})(\text{bpy})_2$  in DMF. On excitation at 460 nm, the steady state emission spectrum of  $\text{Ru}(\text{ap})(\text{bpy})_2$ -decorated SWCNT in DMF revealed a strongly quenched ( $> 98\%$ ) 606-nm photoluminescent peak compared to that of  $\text{Ru}(\text{ap})(\text{bpy})_2$  in DMF (Fig. 10B). Emission spectra were collected after having matched the absorptions, at the 460-nm excitation wavelength, of free  $\text{Ru}(\text{ap})(\text{bpy})_2$  and  $\text{Ru}(\text{ap})(\text{bpy})_2$  grafted onto SWCNT. Excitation at 375 nm showed similar quenching to further confirm the formation of the linked supramolecular electron donor-acceptor complexes between

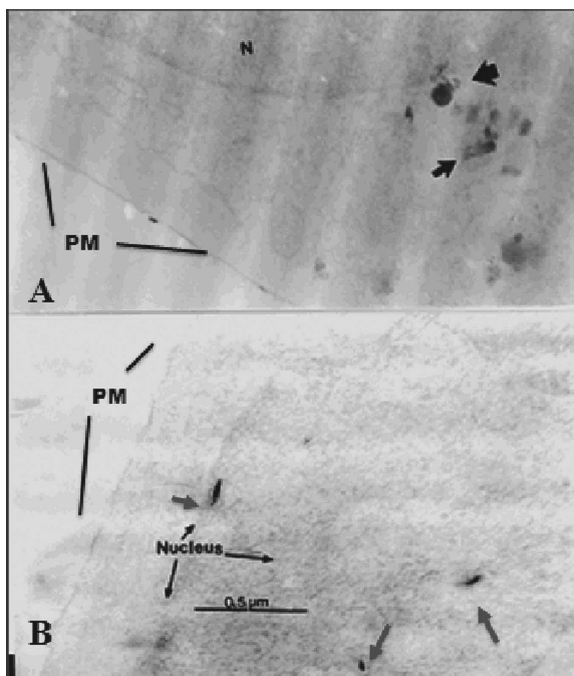


**Fig. 10** Absorbance (A) and emission (B) spectra of  $\text{Ru}(\text{ap})(\text{bpy})_2$  (dotted line) and  $\text{Ru}(\text{ap})(\text{bpy})_2$ -decorated SWCNT (solid line) dispersions in DMF. For the emission spectra, we matched the absorptions, at the 460-nm excitation wavelength, of free  $\text{Ru}(\text{ap})(\text{bpy})_2$  and  $\text{Ru}(\text{ap})(\text{bpy})_2$  grafted onto SWCNT, calculated by subtracting from the absorbance spectrum of the nanostructure that of oxidized SWCNT

the metalloorganic luminophores, which acted as electron-transfer agents, and the carbon nanotubes, which acted as electron acceptors. Addition of free luminophore to the nanocomposite dispersions increased their emission intensities. These increases in emission suggest that, at the low concentrations used, dynamic (collisional) quenching was not responsible for the observed fluorescence quenching, which could only be caused by photo-induced charge injection from the metal-to-ligand charge-transfer (both singlet and triplet) excited states of the luminophore into the conduction band of the SWCNT.

Transmission electron microscope images of fSNB showed uniform diameter ( $13 \pm 1$  nm) silica nanobeads. Absorbance spectra of both free and fSNB-encapsulated  $\text{Ru}(\text{bpy})_3$  in EtOH were characterized by a narrow peak at approximately 290 nm and by a broad plateau at approximately 450 nm, which we attribute to a ligand-to-ligand  $\pi \rightarrow \pi^*$  transition and a  $d_{\text{Ru}} \rightarrow \pi^*$  ligand singlet metal-to-ligand charge-transfer transition, respectively. The peaks in the spectrum of the fSNB in EtOH were slightly red-shifted and broader compared to those of free  $\text{Ru}(\text{bpy})_3$  (Fig. 11A). In steady state experiments, excitation of fSNB in EtOH at 452 nm produced an emission band that was enhanced, red-shifted and broader compared to that

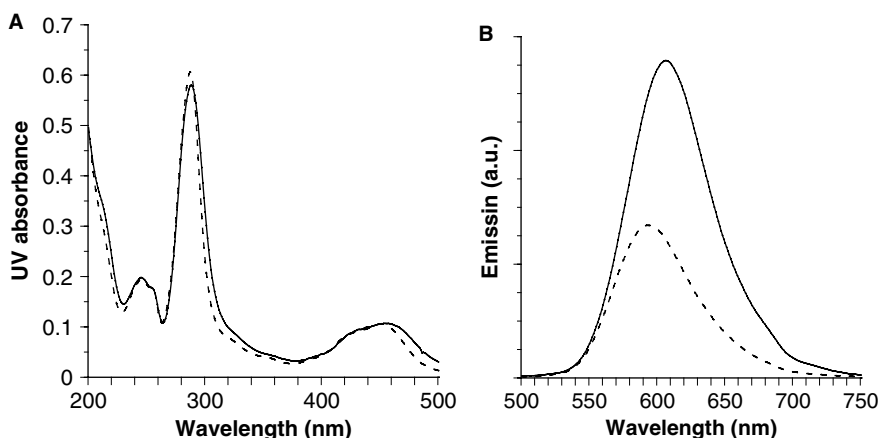


**Fig. 11** Absorbance (**A**) and emission (**B**) spectra of Ru(bpy) (dotted line) and fSNB (solid line) dispersions in EtOH. For the emission spectra, we matched the absorptions, at the 452-nm excitation wavelength, of free Ru(bpy) and fSNB

of Ru(bpy) (Fig. 11B). The emission spectra were collected after having matched the absorptions, at the 452-nm excitation wavelength, of free Ru(bpy) and fSNB. These results suggest that the silica bead network may have affected the electrostatic environment surrounding the entrapped luminophores and that encapsulation protected Ru(bpy) from any dynamic self-quenching caused by collisional encounters.

The absorbance spectra of both fSNB-decorated SWCNT (Fig. 12A) and MWCNT (Fig. 12B) dissolved in EtOH showed broad peaks at approximately the same wavelengths as those from fSNB to confirm that fluorescent nanoparticles decorated the nanotube surfaces (Fig. 12C). The spectroscopic contribution of fSNB grafted onto the CNT surface was calculated by subtracting from the absorbance spectrum of the nanocomposite that of silylated CNT with matching absorption at 900 nm, as the spectroscopic contribution of free fSNB was absent for that wavelength. The peaks in the calculated absorbance spectra of fSNB grafted onto both (both SW and MW) CNT were slightly red-shifted compared to those of free fSNB in EtOH. On excitation at 452 nm, the steady-state emission spectrum of fSNB-decorated CNT exhibited slightly quenched ( $< 5\%$ ), narrower and blue-shifted emission peaks compared to that of free fSNB (Fig. 12D). The emission spectra were collected after having matched the absorptions, at the 452-nm excitation wavelength, of free fSNB and fSNB grafted onto CNT.

The observed slight quenching could be addressed to the error in the calculation of fSNB grafted onto CNT and/or to the electron transfer from the luminophores close to the fSNB silica surface to the CNT. Therefore, the silica host was able to avoid the quenching of the fluorescence due to the charge injection from the metal-to-ligand charge-transfer excited states of the luminophore into the conduction band of the quencher (CNT), leading to the realization of a supramolecular fluorescent nanostructure useful for a large variety of applications ranging from biosensors to

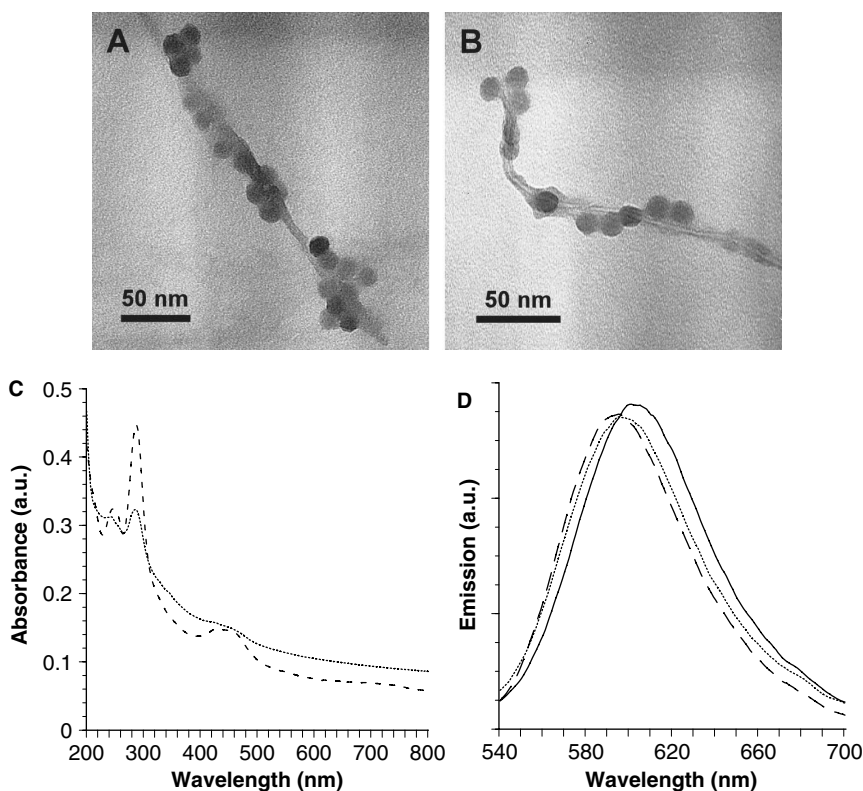


**Fig. 12** Transmission electron microscope images of SWCNT (A) and MWCNT (B) decorated with fluorescent silica nanobeads. C: Absorbance spectra of fSNB-decorated SWCNT (*dashed line*) and fSNB-decorated MWCNT (*dotted line*) dispersions in EtOH. D: Emission spectra of fSNB (*solid line*), fSNB-decorated SWCNT (*dashed line*) and fSNB-decorated MWCNT (*dotted line*) dispersions in EtOH. For the emission spectra, we matched the absorption values at the 452-nm excitation wavelength, of free fSNB and fSNB grafted onto CNT, calculated by subtracting from the absorbance spectrum of the nanocomposite that of silylated CNT

electronics, especially in case of use of pristine full-length CNT that are characterized by intact  $\pi$ -electronic structure.

In summary, we synthesized in [32] three supramolecular nanostructures based on CNT and ruthenium-complex luminophores. The first nanostructure consisted of short oxidized SWCNT covalently decorated by ruthenium-complexes that act as light-harvesting antennae by donating their excited-state electrons to the SWCNT. This nanocomposite represents an excellent donor-acceptor complex, which may be particularly useful for the construction of photovoltaic devices based on metalloorganic luminophores. The second and the third nanostructures consisted of metalloorganic luminophore-doped silica nanobeads covalently linked to short oxidized SWCNT or hydrophobically adsorbed onto full-length MWCNT. In these nanocomposites, the silica network prevented the fluorescence quenching because

excited-state electrons could not be readily donated to the CNT conduction band. Because the physical and chemical properties of the silica nanobeads are so versatile, and the  $\pi$ -electronic structure of the CNT can be kept intact by using a non-destructive modification of the nanotube structure, we consider these nanocomposites to have a promise for a variety of applications ranging from the biosensors to electronics.

## 6 Cellular Toxicity of Carbon Nanotubes

Very little is yet known about the toxicity of CNTs, which exist in many different forms and can be chemically modified and/or functionalized with biomolecules. Pristine single-walled CNTs are extremely hydrophobic tubes of hexagonal carbon (graphene) with diameters as small as 0.4 nm and lengths up to micrometers. Multi-walled CNTs consist of several concentric graphene tubes and diameters of up to 100 nm. These pristine CNTs are chemically inert and insoluble in aqueous media and therefore of little use in biological or medical applications. Due to the hydrophobicity and tendency to aggregate, they are harmful to living cells in culture [33,34].

As we have seen in one of the above sections, for many applications, CNTs are oxidized in strong acid to create hydroxyl and carboxyl groups [35], particularly at their ends, to which biomolecules or other nanomaterials can be coupled [25]. These oxidized CNTs are much more readily dispersed in aqueous solutions and have been coupled to oligonucleotides, proteins, or peptides. Indeed, CNTs have been used as vehicles to deliver macromolecules that are not able pass through the cellular membrane by themselves into cells [36,37].

Since little is yet known about the toxicity of CNTs, particularly of oxidized CNTs, we compared in [38] these two types of CNTs in a number of functional assays with human T lymphocytes, which would be among the first exposed cell types upon intravenous administration of CNTs in therapeutic and diagnostic nanodevices.

We found that, especially for high concentration ( $>1\text{ng}/\text{cell}$ ), CB are less toxic than pristine CNTs, therefore suggesting the relevance of the structure and topology (carbon black is amorphous) on the evaluation of the toxicity of a carbonaceous nanomaterial. Moreover, we found that oxidized CNTs are more toxic than pristine CNTs for both the analyzed concentrations, although they are considered better suited for biological applications. This may well be because they are better dispersed in aqueous solution and therefore reach a higher concentration of free CNTs at similar weight per volume values. We calculated that the less toxic amount of  $40\text{ }\mu\text{g}/\text{ml}$  of CNTs is equal to an order of magnitude of  $10^6$  individual CNTs per cell in our experiments, based on an average length of  $1\text{ }\mu\text{m}$  and a diameter of 40 nm, giving an average molecular mass of  $5 \times 10^9$  Da.

While our results in [38] do not imply that CNTs should be abandoned for biological or medical purposes, our study sets an upper limit for the concentrations of CNTs that can be used. We recommend that CNTs be used at much less than



1 ng/cell and that cell viability and wellbeing be followed carefully with all new forms of CNTs and CNT-containing nanodevices. It is likely that CNT toxicity will depend on many other factors than concentration, including their physical form, their diameter, their length, and the nature of attached molecules or nanomaterials.

## **7 Separation of Fluorescent Material from Single Wall Carbon Nanotubes**

For biotechnological uses [39], a high level of purity is required to avoid undesired toxic effects from impurities. Contaminants in SWNT can be classified as carbonaceous (amorphous carbon and graphitic nanoparticles) and metallic (typically transition metal catalysts). It is well documented that nickel, which in combination with yttrium is used as a catalyst in the production of arc-discharged nanotubes, is cytotoxic [40]. Common SWNT purification methods based on oxidation (nitric acid and/or air) have the potential disadvantage of modifying the CNT by introducing functional groups and defects. Other less rigorous purification techniques rely upon filtration, centrifugation and chromatography. Recently, electrophoresis of nitric acid-treated arc-discharged SWNT was used to separate tubular carbon from fluorescent nanoparticles [41].

As we reported in [42], fluorescent nanoparticles were isolated from both pristine and nitric acid-oxidized commercially available carbon nanotubes that had been produced by an electric arc method. The pristine and oxidized carbon nanotube-derived fluorescent nanoparticles exhibited a molecular-weight-dependent photoluminescence in the violet-blue and blue to yellowish-green ranges, respectively. The molecular weight dependency of the photoluminescence was strongly related to the specific supplier. We analyzed the composition and morphology of the fluorescent nanoparticles derived from pristine and oxidized nanotubes from one supplier. We found that the isolated fluorescent materials were mainly composed of calcium and zinc. Moreover, the pristine carbon nanotube-derived fluorescent nanoparticles were hydrophobic and had a narrow distribution of maximal lateral dimension. In contrast, the oxidized carbon nanotube-derived fluorescent nanoparticles were superficially oxidized and/or coated by a thin carbon layer, had the ability to aggregate when dispersed in water, and exhibited a broader distribution of maximal lateral dimension.

The first sample we treated (pNT) was composed of as-prepared nanotubes (AP-SWNT), purified by air oxidation, and the second one (oxNT) was obtained by nitric acid oxidation of AP-SWNT. Both samples had a carbon content in the 80–90 wt-% range and approximately 10 wt-% nickel/yttrium catalyst (4:1). Samples of graphite, carbon black, pNT and oxNT samples were dispersed in aqueous sodium dodecyl sulfate (SDS, 1 wt-%) surfactant using an ultrasonic bath.

Our spectral results reported in [42] may be explained by the presence of fluorescent particles (FP) with variable dimensions and chemistries in the NT samples. The predominant FP in pNT had a mean mw below 30 kDa and exhibited mainly

violet-blue photoluminescence and excitation at 315 nm. In contrast, in the fourth fraction (30 kDa–100 kDa), these spectral properties were weaker. All four fractions exhibited 450-nm and 485-nm photoluminescence on 365-nm excitation. The FP in the pNT sample may originate from a nickel and yttrium-containing catalyst that had been covered by a few thin layers of metal oxide and/or carbide during the synthetic process, as was reported by Martinez et al. [43].

Our results suggest that the presence of the FP contaminants in these samples as aggregates or occlusions on NT walls led to quenching of their photoluminescence. Sonication in the presence of the surfactant SDS was able to enrich the solution in micelle-embedded FP. To support this argument, Martinez et al. found that the material encasing the catalyst accompanying nitric acid-oxidized NT masked the metal core from detection by surface-sensitive techniques such as X-ray photoelectron spectroscopy. Their study may also explain the results of Xu et al., who, despite using energy-dispersive X-ray spectroscopy, were unable to discern any metal in the fluorescent electrophoresis fractions from oxidized SWNT [41].

In our study [42], the FP from the oxNT exhibited more size-dependence in their photoluminescence, which ranged from greenish-blue to orange, than those from the pNT. The oxNT FP were also more hydrophilic, probably because their carbon shells became carboxylated on oxidation, as was reported by Xu et al. In addition, our spectra suggest the presence of a less-abundant FP fraction, which had a mean mw below 3 kDa and 425-nm emission peaks on excitation at 315 nm. On the basis of comparing these spectral properties with those of the FP from pNT, FP from the oxNT also contained fluorescent components derived from the pNT.

The above findings led us to design a new SWNT purification method. Each dispersed NT sample was ultracentrifuged (as described above). The pellet was subjected to three additional rounds of dispersion in vehicle, sonication for 5 minutes and ultracentrifugation. A spectrum indicative of few residual FP was exhibited by oxNT-in-water. The spectra of the pNT-in-SDS and oxNT-in-SDS samples resembled that of graphite to demonstrate the absence of fluorescent contaminants. These results suggest that, in addition to amplifying FP photoluminescence, the surfactant facilitated FP removal. In summary, we now have a simple route consisting of surfactant-assisted dispersal followed by ultracentrifugation for removing FP contaminants from both pristine and nitric acid-treated SWNT.

In summary, we isolated, fractionated by molecular weight and characterized FP from pCNT and oxCNT received from several suppliers. These FP were responsible for the photoluminescence of electric arc-produced CNT in the visible range and were likely composed of impurities that were present in the graphite rods used for the production of the CNT. Spectroscopic analysis of the samples revealed some common supplier-independent features, specifically that the FP derived from the pCNT exhibited a violet-blue photoluminescence, whereas the FP derived from the oxCNT exhibited photoluminescence ranging from blue to yellowish-green. In contrast, the molecular weight dependency for both the pristine and oxidized CNT-derived fractions was strongly related to the specific supplier. This can be explained by differing fabrication processes leading to different physical and chemical aggregation of the impurities present in the graphite rod. We recorded HRTEM

images and EDX analysis of the FP isolated from the CNT (Carbon Solutions, Inc.)-derived molecular weight fractions. The FP derived from the pCNT exhibited a narrow range in width, whereas the FP derived from the oxCNT were larger, had a broader width range, and formed hydrophilic aggregates in water. Moreover, EDX analysis of the fractions from the oxCNT-in-water supernate suggested that their FP were superficially oxidized and/or coated by a thin carbon layer.

## 8 Conclusions

The field of nanoscience has been witnessing a rapid growth in the last decade. Recently, more and more, the attention of the community of nanoscientists has been focusing on technological applications. Nanotechnology has been emerging as an enabling technology, with high potential impact on virtually all fields of mankind activity (industrial, health-related, biomedical, environmental, economy, politics, etc.), yielding high expectations for a solution to the main needs of society, although having to address open issues with respect to its sustainability and compatibility.

The fields of application of the research in nanoscience include aerospace, defense, national security, electronics, biology and medicine. There has been a significant progress in understanding achieved in recent years, both from the theoretical and experimental point of view, along with a strong interest to assess the current state of the art of this fast growing field, stimulating, at the same time, research collaboration among the different stakeholders in the area of nanoscience and the corresponding technological applications, prompting possibly the organization and presentation of joint projects in the near future involving both industry and public research.

In the present article, we focused in particular on the biological and medical fields and described current and possible future developments in nanotechnological applications in such areas. Nanostructured, composite materials for drug delivery, biosensors, diagnostics and tumor therapy were reviewed here as examples. Carbon nanotubes were discussed as a primary example of emerging nanomaterials for many of the abovementioned applications.

**Acknowledgements** The author acknowledges members of his group for nanotechnology at INFN-LNF and collaborators for their work on the developments discussed in this article.

## References

1. S. Iijima, *Nature*, 1991, 354, 56.
2. M.S. Dresselhaus, G. Dresselhaus, P. Avouris (Eds.), 2001. *Carbon nanotubes: Synthesis, structure, properties and applications*. Springer, Berlin.
3. <http://www.germanyinfo.org/relaunch/info/publications/week/2003/030613/misc2.html>

4. R. Hergt, R. Hiergeist, J. Hilger, W.A. Kaiser, Y. Lapatnikov, S. Margel, and U. Richter, *J. Magnetism and Magnetic Materials*, 2004, 270, 345.
5. A. Ito, F. Matsuoaka, H. Honda, and T. Kobayashi, *Cancer Immunology Immunotherapy*, 2004, 53 (1), 26.
6. D.P. O'Neal, L.R. Hirsch, N.J. Halas, J.D. Payne, and J.L. West, *Cancer Letters*, 2004, 209, 171.
7. D. Luo, E. Han, N. Belcheva and W.M. Saltzman, *J. Controlled Release*, 2004, 95, 333.
8. A.K. Salem, P.C. Searson and K.W. Leong, *Nat. Mater.*, 2003, 2, 668.
9. G.F. Paciotti, L. Myer, D. Weinreich, D. Goia, N. Pavel, R.E. McLaughlin and L. Tamarkin, *Drug Deliv.*, 2004, 11, 169.
10. K.S. Soppimath, T.M. Aminabhavi, A.R. Kulkarni and W.E. Rudzinski, *J. Controlled Release*, 2001, 70, 1.
11. P. Nednoor, M. Capaccio, V.G. Gavalas, M.S. Meier, J.E. Anthony and L.G. Bachas, *Bioconjug. Chem.*, 2004, 15, 12
12. T. Konno, J. Watanabe and K. Ishihara, *Biomacromolecules*, 2004, 5, 342.
13. X.L. Luo, J.J. Xu, W. Zhao and H.Y. Chen, *Biosens. Bioelectron.*, 2004, 19, 1295
14. S. Hrapovic, Y. Liu, K. B. Male and J.H. Luong, *Anal. Chem.*, 2004, 76, 1083.
15. M.C. Daniel and D. Astruc, *Chem. Rev.*, 2004, 104, 293.
16. W. Tan, K. Wang, X. He, X.J. Zhao, T. Drake, L. Wang and R.P. Bagwe, *Med. Res. Rev.*, 2004, 24, 621
17. S. Santra, P. Zhang, K.Wang, R. Tapeç and W. Tan, *Anal. Chem.*, 2001, 73, 4988
18. initial He, K. Wang, W. Tan, B. Liu, X. Lin, C. He, D. Li, S. Huang and J. Li, *J. Am. Chem. Soc.*, 2003, 125, 7168.
19. T. Seeger, Ph. Redlich, N. Grobert, M. Terrones, D.R.M. Walton, H.W. Kroto and M. Rühle, *Chem. Phys. Lett.*, 2001, 339, 41
20. E. Whitsitt and A. R. Barron, *Nano Lett.*, 2003, 3, 775.
21. H. Kim and W. Sigmund, *Appl. Phys. Lett.*, 2002, 81, 2085.
22. J.M. Haremza, M.A. Hahn and T.D. Krauss, *Nano Lett.*, 2002, 2, 1253.
23. S. Ravindran, S. Chaudhary, B. Colburn, M. Ozkan and C. S. Ozkan, *Nano Lett.*, 2003, 3, 447.
24. S. Lee and W. Sigmund, *Chem. Commun.*, 2003, 6, 780.
25. J. Sun, L. Gao and M. Iwasa, *Chem. Commun.*, 2004, 7, 832.
26. Massimo Bottini, Lutz Tautz, Huong Huynh, Edvard Monosov, Nunzio Bottini, Marcia I. Dawson, Stefano Bellucci and Tomas Mustelin, *Chem. Commun*, 2005, 6, 758.
27. J. Liu, A.G. Rinzler, H. Dai, J.H. Hafner, R.K. Bradley, P.J. Boul, A. Lu, T. Iverson, K. Shelimov, C.B. Huffman, F. Rodriguez-Macias, Y. Shon, T.R. Lee, D.T. Colbert and R.E. Smalley, *Science*, 1998, 280, 1253.
28. J. Esquena, Th. F. Tadros, K. Kostarelos and C. Solans, *Langmuir*, 1997, 13, 6400
29. F.J. Arriagada and K. Osseo-Asare, *J. Colloid Interface Sci.*, 1999, 211, 210.
30. R.P. Bagwe, C. Yang, L.R. Hilliard and W. Tan, *Langmuir*, 2004, 20, 8336.
31. H.H. Yang, S.Q. Zhang, X.L. Chen, Z.X. Zhuang, J.G. Xu and X.R. Wang, *Anal. Chem.*, 2004, 76, 1316.
32. G. Fiandaca, E. Vitranò and A. Cupane, *Biopolymers*, 2004, 74, 55.
33. Massimo Bottini, Andrea Magrini, Almerinda Di Venere, Stefano Bellucci, Marcia I. Dawson, Nicola Rosato, Antonio Bergamaschi, and Tomas Mustelin, *J. Nanosci. Nanotechnol.*, 2006, 6, 1381.
34. Cui, D., Tian, F., Ozkan, C.S., Wang, M., Gao, H., *Toxicol. Lett.*, 2005, 155, 73
35. Monteiro-Riviere, N.A., Nemanich, R.J., Inman, A.O., Wang, Y.Y., Riviere, J.E., *Toxicol. Lett.*, 2005, 155, 377.
36. Liu, J., Rinzler, A.G., Dai, H., Hafner, J.H., Bradley, R.K., Boul, P.J., Lu, A., Iverson, T., Shelimov, K., Huffman, C.B., Rodriguez-Macias, F., Shon, Y.S., Lee, T.R., Colbert, D.T., Smalley, R.E., *Science*, 1998, 280, 1253.
37. Pantarotto, D., Briand, J.P., Prato, M., Bianco, A., *Chem. Commun.*, 2004, 16 Shi Kam, N.W., Jessop, T.C., Wender, P.A., Dai, H., *J. Am. Chem. Soc.*, 2004, 126, 6850.
38. Bottini M, Bruckner S, Nika K, Bottini N, Bellucci S, Magrini A, Bergamaschi A, Mustelin T., *Toxicol Lett.*, 2006, 160, 121.

39. Baughman RH, Zakhidov AA, de Heer WA., *Science*, 2002, 297, 787.
40. Pulido MD, Parrish AR., *Mutat. Res.*, 2003, 533, 227.
41. Xu X, Ray R, Gu Y, Ploehn HJ, Gearheart L, Raker K, Scrivens WA, *J. Am. Chem. Soc.*, 2004, 126, 12736.
42. Massimo Bottini, Chidambara Balasubramanian, Marcia I Dawson, Antonio Bergamaschi, Stefano Bellucci, Tomas Mustelin, *J Phys Chem B Condens Matter Mater Surf Interfaces Biophys.*, 2006, 110, 831
43. Martinez MT, Callejas MA, Benito AM., Maser WK, Cochet M, Andres JM, Schreiber J, Chauvet O, Fierro JL., *Chem. Commun*, 2002, 7(9), 1000.



Nanoparticles and Nanodevices in Biological  
Applications

The INFN Lectures - Vol I

Bellucci, S. (Ed.)

2009, XII, 198 p. 153 illus., 7 illus. in color., Hardcover

ISBN: 978-3-540-70943-5